Journal of Power Sources 195 (2010) 7644–7648

Contents lists available at ScienceDirect

Journal of Power Sources

journal homepage: www.elsevier.com/locate/jpowsour

Short communication

Depth profile analysis of a cycled lithium ion manganese oxide battery electrode via the valence state of manganese, with soft X-ray emission spectroscopy

Artur Braun[a,b,*], Hongxin Wang[c,d], Tobias Funk[c], Soenke Seifert[e], Elton J. Cairns[a,f]

[a] Environmental Energy Technologies Division, Ernest Orlando Lawrence Berkeley National Laboratory, Berkeley, CA 94720, United States
[b] Laboratory for High Performance Ceramics, Empa, Swiss Federal Laboratories for Materials Science and Technology, CH-8600 Dübendorf, Switzerland
[c] Physical Biosciences Division, Ernest Orlando Lawrence Berkeley National Laboratory, Berkeley, CA 94720, United States
[d] Department of Applied Science, University of California, Davis, CA 95616, United States
[e] Advanced Photon Source, Argonne National Laboratory, Argonne, IL 60439, United States
[f] Department of Chemical Engineering, University of California, Berkeley, CA 94720, United States

ARTICLE INFO

Article history:
Received 19 April 2010
Received in revised form 24 May 2010
Accepted 25 May 2010
Available online 31 May 2010

Keywords:
Lithium battery
X-ray spectroscopy
Depth profile
Manganese oxide
Valence state

ABSTRACT

A 50-μm thick lithium manganese oxide (parent material $LiMn_2O_4$) battery electrode (positive electrode; cathode) was charged, slightly discharged and then sliced with a scotch tape test-type method. A selected number of slices was then subject to synchrotron soft X-ray emission spectroscopy near the Mn $L_{\alpha,\beta}$ emission lines in order to determine changes in the oxidation state of the manganese as a function of sampling depth. The emission spectra showed a minute yet noticeable and systematic chemical shift of up to 0.25 eV between the layer near the current collector and the layer near the electrolyte separator. The average manganese oxidation state near the separator was smaller than the average oxidation state in the interior of the electrode, or near the current collector. Since the data provide an oxidation state depth profile of the cathode, a Li^+ depth profile can be inferred. This method provides information on the spatial chemical inhomogeneity of electrodes prior to and after electrochemical cycling, and thus can aid in degradation studies.

1. Introduction

"Where does the lithium go?" has been an important question [1] since performance loss and electrode degradation have become pressing issues in lithium battery engineering and research. Naturally, the search for lithium requires appropriate detection techniques with a particular spatial resolving power. When an electrode sustains state-of-charge differences in different locations, then this is evidence for loss of electronic or electrolytic contact with parts of the electrode. In the search for lithium, not only information on the presence or absence of lithium is important, but also information on whether lithium is chemically bound to the electrode host material, or not.

To briefly explain the difficulty of this seemingly simple task, consider for example the two following potential approaches: (i) Nuclear magnetic resonance (NMR) spectroscopy is a method with a very good chemical sensitivity for lithium, allowing one to distinguish the lithium in different molecular environments [2]. NMR typically requires large amounts of material, is normally an ex situ technique, and thus does not allow for spatial resolution in the micrometer range. Electron microscopy allows for high spatial, even atomic resolution [3], but is of little use for chemical information. We have recently succeeded in presenting a suite of Li(1s) near edge X-ray absorption fine structure (NEXAFS) spectra of representative lithium ion battery component materials [4], but this method alone is not yet feasible for spatially resolved information. Here we present an indirect way of determining the concentration of lithium across the thickness of the positive electrode via direct determination of the Mn oxidation state. The electrode is sliced into sections of a few micrometer thickness with a scotch tape test-type technique. The electrode material sticking on the tape is then subject to X-ray emission spectroscopy near the manganese $L_{\alpha,\beta}$ emission lines, generally allowing for chemical speciation of the manganese, particularly determination of the oxidation state by evaluation of the chemical shift. The chemical shift in X-ray absorption or emission spectra has been shown to be a valuable approach for the identification of chemical inhomogeneities in lithium battery materials, allowing statements on the surface and bulk chemistry in the materials [5]. By consideration of the stoichiometry of lithium manganate under a particular state-of-charge, which stoichiometrically can be expressed as $Li_{(1-x)}[Mn^{3+}]_{(1-x)}[Mn^{4+}]_{(1+x)}O_4$, and by the

* Corresponding author at: Laboratory for High Performance Ceramics, Empa, Swiss Federal Laboratories for Materials Science and Technology, CH-8600 Dübendorf, Switzerland. Tel.: +41 44 823 4850; fax: +41 44 823 4150.
E-mail address: artur.braun@alumni.ethz.ch (A. Braun).

0378-7753/$ – see front matter © 2010 Elsevier B.V. All rights reserved.
doi:10.1016/j.jpowsour.2010.05.053

corresponding changes in the manganese valence state, information on the Li^+ is indirectly obtained.

In the present study, lithium manganate was investigated with soft X-ray L-edge emission spectroscopy. The manganate was present in the form of an electrode from the parent compound $LiMn_2O_4$, which was electrochemically charged to 4.30 V, then slightly discharged [6] in situ in an X-ray spectroelectrochemical reaction cell [7] and thereafter sliced for depth profile analysis. With this study we found that it is feasible to monitor oxidation state vs. thickness profiles of electrodes and thus information about the spatial chemical homogeneity of the electrodes prior to and after cycling.

2. Experimental equipment and procedures

The parent cathode material was prepared from a stoichiometric mixture of Li_2CO_3 (J.T. Baker), MnO_2 (Japan Metals, CMD). The mixture was fired at 850 °C in air for 20 h, then removed from the furnace and cooled down in ambient atmosphere, yielding nominally $LiMn_2O_4$ [8]. The resulting spinel powder had a primary particle size of around 1 μm and was mixed with graphite (Timcal, Switzerland), Shawinigan Black, and PVDF binder. The slurry was cast on 25 μm thick aluminum foil and subsequently dried at 423 K, which resulted in an electrode with a spinel layer thickness of around 50 μm, containing spinel to 80 wt% (9.25 ± 1.25 mg) [5,6].

This electrode was assembled in an X-ray spectroelectrochemical in situ cell [7] and charged at a current density of 50 μA cm^{-2} until the open circuit potential of 4.3 V was reached, with a charge of 88.8 mA min (1.48 mAh). At this state, the average Mn oxidation state is Mn^{4+}. Then the cell was rapidly partially discharged at 200 μA cm^{-2} back to the 70 mA min level, which corresponds, in linear approximation, to an average change of valence from $Mn^{3.5+}$ to Mn^{4+} to $Mn^{3.9+}$. The change of the oxidation state of the entire electrode was monitored operando in an in situ spectroelectrochemical cell with hard X-ray absorption near edge spectroscopy (XANES) at the Mn K-shell absorption edge [6]. The cell was then disassembled in dry Ar atmosphere, where the cathode assembly was rinsed in acetonitrile seven times in order to remove electrolyte and potential excess lithium [9], and the assembly dried in ambient atmosphere on a microbalance until no weight change was noticed. Removal of the $LiPF_6$-containing electrolyte is critical because it may form malign HF with ambient H_2O in the atmosphere [10]. However, one cannot entirely rule out that evidence of potential operational damage that was made to the cell is being removed with this acetonitrile rinsing.

The cycled and uncycled electrode material was subject to powder X-ray diffraction (Siemens D5000 diffractometer with Cu Kα radiation), step size $2\Theta = 0.1°$, in the range from 1° to 60°.

The dried assembly was then weighed and subsequently firmly pressed onto a sticky piece Kapton tape, which had been weighed before. The tape was removed and virtually contained the entire spinel material, whereas only traces of spinel remained on the aluminum current collector. Another Kapton tape was then pressed on the spinel sticking on the first Kapton tape, and immediately removed again, so that a thin layer of spinel stuck on the second Kapton tape, both of which were then independently weighed on the balance. This procedure was repeated with more Kapton tapes until the first Kapton tape weighed around as much as either of the other Kapton tapes. We thus had a suite of 12 Kapton tapes with known amount of spinel coverage (milligram), which allowed us to relate every layer of spinel on each Kapton tape to a particular depth in the electrode.

This technique allows to reproducibly "slice" a 50-μm thick electrode into 10–20 layers. We have sliced the sample under consideration into 12 parts. Using a high precision laboratory balance it was possible to assign each slice to a relative depth position in the electrode, with an accuracy of about 10%. Five of these slices were subjected to manganese L_α emission spectroscopy at Beamline 8.0.1 at the Advanced Light Source with excitation photon energy of 680 eV. Every sample was measured 4 times with an exposure time of 900 s each. The spectra for each sample were averaged and normalized.

Note that because the spinel material was fixed on a non-conducting Kapton tape, electrical charging effects may impede soft X-ray absorption experiments with electron yield detection techniques. Also, it is important that the spinel layers are not probed with respect to the surface, but with a more bulk sensitive detection technique. We have previously shown that the oxidation state of Mn on or near the surface may differ from that in the bulk [5]. We therefore decided to employ X-ray emission spectroscopy (XES) with photon yield detection (photon in–photon out mode).

3. Results and discussion

The charging and discharging treatment of the electrode in the in-situ cell is shown in Fig. 1 [7]. Due to the stoichiometry of the prepared electrode, which we are confident is $LiMn_2O_4$, we can assume that the charging begins with an average Mn oxidation state of $Mn^{3.5+}$ and approaches the average oxidation state of Mn^{4+} at around 1830 min of charging and 88.8 mA min. The cell was then discharged for 70 mA min and disconnected. We estimate an average Mn oxidation state of slightly below $Mn^{3.9+}$.

While the Mn sites near the current collector tend to be reduced during the discharging step after charging, global demand electroneutrality would require the Li^+ to migrate into the electrode from the separator side, creating a local polarization. This would probably relax back in the sense of an equilibration. However, in the absence of electrolyte, the movement of the lithium is not very fast, even if the electron-hopping between Mn^{4+} and Mn^{3+} sites in the solid-state is not a slow process.

The charging and subsequent partial discharging is paralleled by the evolution of the X-ray absorption near edge structure (XANES) spectra obtained at the manganese K-shell absorption edge near

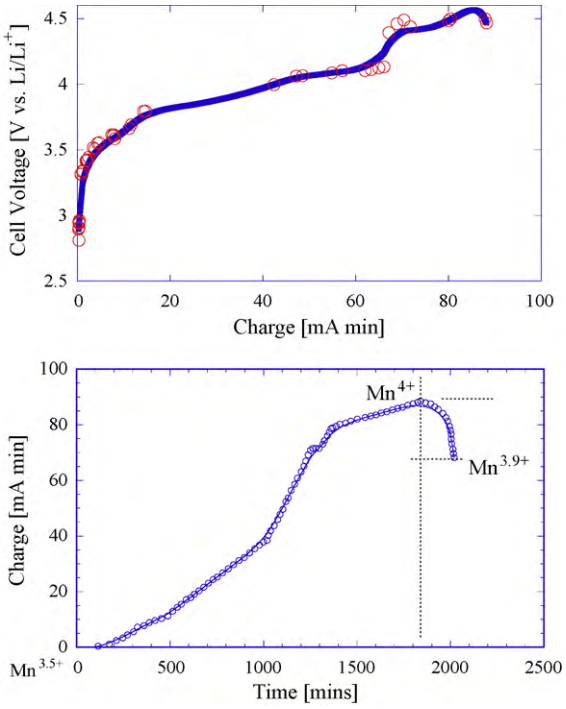

Fig. 1. Charging and discharging characteristic of the electrode contained in the in situ cell.

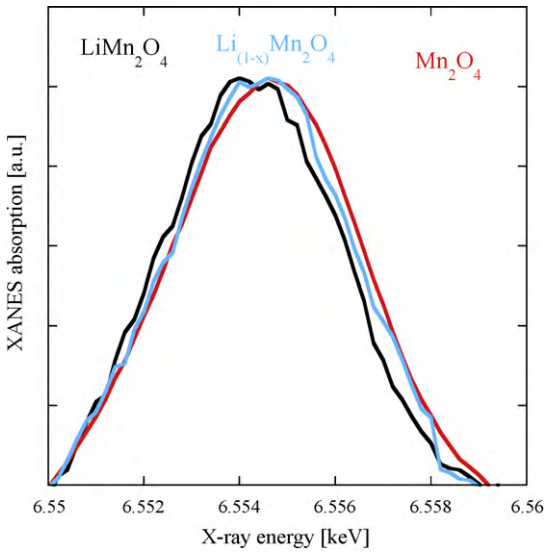

Fig. 2. Manganese white lines of the K-shell absorption edge of the in situ cell loaded with spinel electrode prior to charging, after charging and after slight rapid discharging.

6540 eV. The white line range of the XANES spectra is shown in Fig. 2 [6], which shows the manganese white lines of the K-shell absorption edge of the in situ cell loaded with spinel electrode prior to charging, after charging and after slight rapid discharging. The white line of the uncycled cell (black spectrum) has the lowest energy position, whereas the spectrum of the fully charged cell (red) has the highest energy position. This chemical shift of the spectra of around 0.5 eV provides circumstantial support that the manganese has been oxidized during charging, i.e. from an average $Mn^{3.5+}$ oxidation state to a Mn^{4+} oxidation state. The spectrum in between (light blue color) was recorded when the cell was slightly discharged and supports the idea that the average oxidation state of Mn^{4+} after charging became reduced to just below $Mn^{3.9+}$ after the 70 mA min discharge.

This electrochemical treatment has caused significant changes in the crystal structure of the electrode, as can be seen in the X-ray diffractogram of the electrode in the uncycled and cycled (charged, and then slightly discharged) state, Fig. 3.

First, we notice that the cycled electrode produces a larger incoherent scattering background than the uncycled electrode. In addition we notice a very small shift of the Bragg reflections in the diffractogram towards larger Bragg angles, suggesting the anticipated contraction of the crystal lattice upon extraction of lithium due to charging. We have determined the crystallite size from the full width at half maximum of Bragg reflexes with the Scherrer equation and found that charging reduced the crystallite size significantly, see Table 1. For example, the length of the crystallite in the (1 1 1) direction changed from 281 nm to 219 nm after the charging and slight discharging. The (0 0 4) reflection actually reverses both intensity ratios upon electrochemical treatment, but since this is a double peak, the accuracy of the Scherrer analysis for this peak is questionable. Comparison of both diffractograms confirms that the electrode underwent noticeable pathogenesis during the one-time charging.

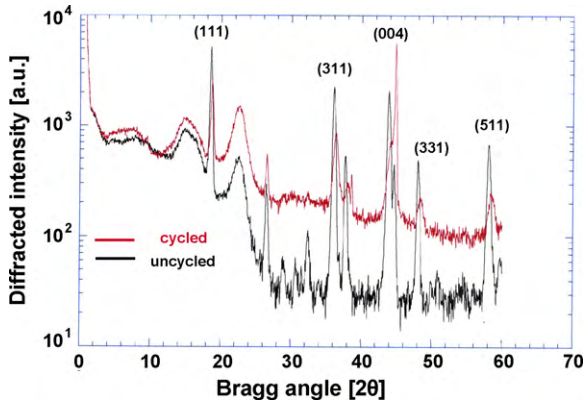

Fig. 3. X-ray diffractogram (Cu Kα) of the non-cycled (bottom, black) and cycled electrode (top, red). (For interpretation of the references to color in this figure legend, the reader is referred to the web version of the article.)

Table 1
Crystallite size for uncycled and cycled electrode material as obtained by the Scherrer equation.

[h k l]	FWHM [2θ]	Position [2θ]	Crystallite size [nm]
(1 1 1) Uncycled	0.298	18.6	281
(1 1 1) Cycled	0.383	18.6	219
(3 1 1) Uncycled	0.451	36.05	218
(3 1 1) Cycled	0.780	36.30	126
(0 0 4) Uncycled (double peak)	0.541	43.85	204
(0 0 4) Cycled (double peak)	0.211	44.85	531
(3 3 1) Uncycled	0.384	48.00	309
(3 3 1) Cycled	0.876	48.35	137
(5 1 1) Uncycled	0.520	58.05	289
(5 1 1) Cycled	0.930	58.49	163

Fig. 4a shows the $L_{\alpha 1,2}$ and L_{β} emission lines at around 645 eV and 655 eV, respectively, for the five spinel samples on Kapton tape sampled at five different depth positions 2,5,7, 10, and 11 in the cathode. Minor, but systematic changes are observed in the range between 635 eV and 650 eV. The spectra are shifted by each other, which is particularly visible between 640 eV and 645 eV. The material sampled at position 2 is closer to the aluminum current collector, whereas the material sampled at position 11 is closer to the face of the cathode, next to the separator with electrolyte filling. Positions 5, 7, and 10 are in between. The $L_{\alpha 1,2}$ peaks show clearly the double peak structure with maxima at about 643.5 eV and 645.5 eV. Close inspection of the magnified region in Fig. 4b shows that the spectra from positions 2, 5, and 7 have that maximum at 645.5 eV, whereas material sampled at positions 10 and 11 have that maximum at 645.9 eV. The maximum for the $L_{\alpha 1,2}$ at around 643.5 eV cannot be quantified so easily, because its resemblance of a shoulder rather than a clear maximum.

The emission spectra reflect the occupied Mn 3d states and represent in this particular case the transitions from Mn 3d states to Mn 2p states. The fine structures visible in the magnification in Fig. 4b have their origin possibly in orbital and spin details, but the resolution of the spectra is not sufficient for quantitative analysis other than chemical shift. The exact interpretation of the Mn 2p spectrum is complicated due to multiple splitting of the Mn^{3+} and Mn^{4+} present in the samples [11]. We see that the spectra for sample positions 2 and 5 are at generally lower energy positions than the other spectra. Generally, in photoemission spectroscopy, a shift of spectral intensity towards lower X-ray energy is indicative of oxidation, and a shift towards higher X-ray energy indicative of reduction of the probed moieties [12].

In order to quantify the chemical shift of emission spectra, such as for our cathode material, and to relate them to the specific properties of the sample position, we compute the first statistical moment $\langle E \rangle$ of the spectral intensity by weighed integration (compare Refs. [5,6]) in the energy range from 635 eV to 665 eV:

$$\langle E \rangle = \frac{\int_{635}^{665} I(E) \cdot E \, dE}{\int_{635}^{665} I(E) \, dE}.$$

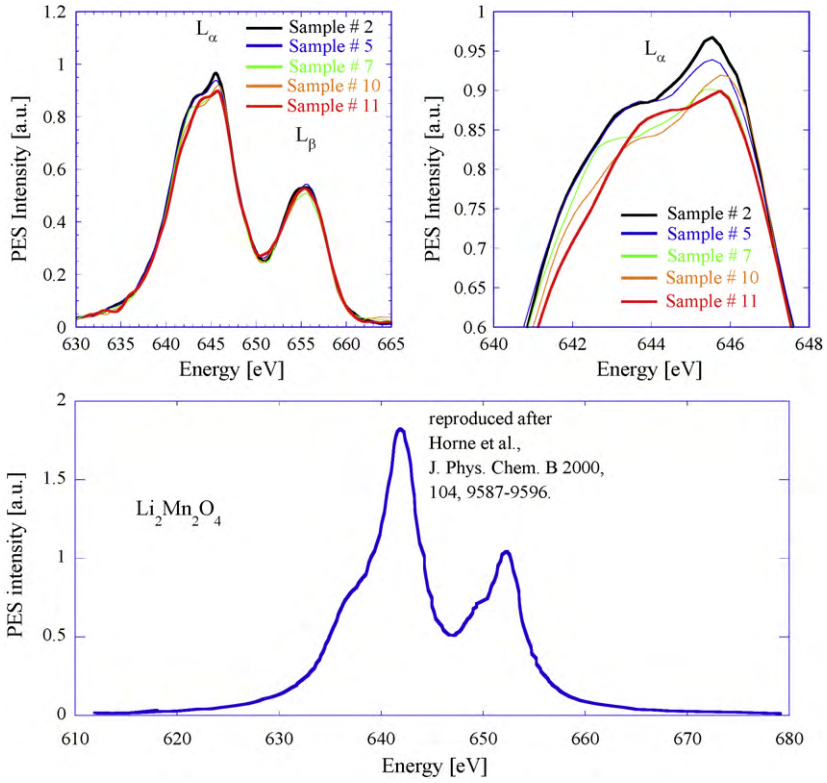

Fig. 4. Left panel: L-edge emission spectra obtained from five sample slices of one electrode. Right panel: magnification of the spectra in the energy range from 640 eV to 648 eV. Bottom: Spectrum of $Li_2Mn_2O_4$, reproduced after Ref. [13]. In this highly lithiated sample Mn exists as Mn^{3+} – the sharp peak at the Lα line is very enhanced compared to our sample.

The manganese in $LiMn_2O_4$ spinel is present in two oxidation states: Mn^{3+} and Mn^{4+}. Upon charging of the cell, a major part of the lithium (about 90%) is electrochemically removed from the spinel lattice, with the result that the Mn^{3+} is oxidized to Mn^{4+}. The stoichiometry of the cathode material at a particular state-of-charge can be written stoichiometrically as $Li_{(1-x)}[Mn^{3+}]_{(1-x)}[Mn^{4+}]_{(1+x)}O_4$. The Li^+ concentration and Mn^{3+} concentration should thus evolve correspondingly. Naturally, if the electrode was rested for a very long time, the difference in the Mn oxidation state disappear by itself because the electrode should relax and come to a single state-of-charge in all electrode parts.

Comparison with the spectrum of $Li_2Mn_2O_4$ in Figs. 4 and 5 in Ref. [13], which is reproduced in our Fig. 4 – in this highly lithiated sample Mn exists as Mn^{3+} – the sharp peak at the L_α line is very enhanced compared to our sample. The spectra of samples from positions 10 to 11 have a particularly low intensity feature at this energy position, confirming that we have predominantly Mn^{4+} species in our sample. This reaction should take place more pronounced at the current collector site of the electrode, because the resistance of the pathway to the current collector is lower there. At the separator site this reaction should take place more slowly. One therefore expects that – after charging – at the current collector there should be a higher concentration of Mn^{4+} than at the separator site. This expectation is confirmed in our experiment, as schematically displayed in Fig. 5. The sketch shows the lateral cross-section of one half cell, in particular the aluminum current collector on the left, which meets the spinel electrode at the position $x = 0$. In the center, the spinel electrodes extends from $x = 0$ to $x = 50\,\mu m$, which is the sample top and faces the separator. On the abscissa, the first moment $\langle E \rangle$ of the spectra is plotted. The abscissa can be directly translated into relative Li^+ concentration vs. sampling distance z.

Samples taken from the current collector site of the electrode assembly have spectra which are shifted towards lower energies, and they have a smaller first moment $\langle E \rangle$ than the spectra from samples which are further away from the current collector.

Note that in our method, any excess lithium in the electrolyte and in pores in the spinel grains would not cause a chemical shift of the manganese and thus would not overshadow any effect on the Li^+ chemically bound to the manganate. This is a distinct advantage compared to other techniques, which are element specific, but not sensitive to the molecular environment of species. Also, our method is particularly applicable to standard electrodes with thicknesses from 10 μm to 100 μm. Here, sputtering techniques for depth profiling would be impractical.

There exist a number of recent works in which researchers have tried to derive concentration profiles of Li and other elements by

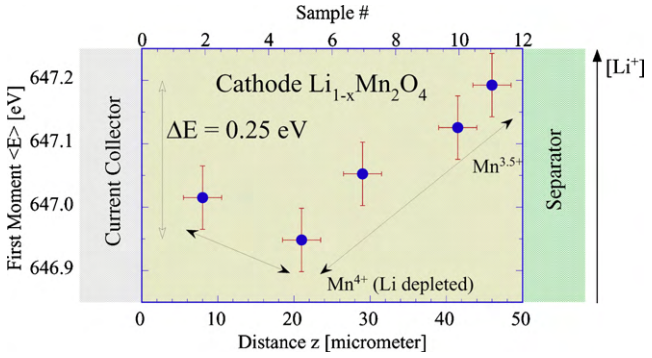

Fig. 5. Schematic of a battery half cell, with inscribed first moment $\langle E \rangle$ of the L_α and L_β emission peak vs. the sample position.

various experimental techniques. It is not in every case possible to directly compare their results with ours because not the same samples were used in terms of stoichiometry, thickness, and equilibration after electrochemical treatment. Reddy et al. [15] have applied Rutherford backscattering and nuclear reaction analysis to probe Li and other elements in a 350 nm thin electrode. Their results show a linear concentration profile of Li with increasing thickness of the electrode, whereas Ni, V and oxygen have a constant profile in this range in the pristine electrode. It remains unclear why Li shows a linear variation across the thickness, then.

Swiatowska et al. [16] have studied Li intercalated in thin V_2O_5 electrode films with X-ray photoelectron spectroscopy (XPS) and time-of-flight secondary ion mass spectroscopy (ToF-SIMS). Depth profiles were obtained by measuring the intensity of prominent peaks in the spectrum as a function of sputtering time. Comparison between two profiles was made possible by normalizing the Li signal to the V signal, assuming the samples were homogeneous and similar prior to Li intercalation. While their study aims particularly at distinguishing different V species for intercalability (V_2O_5 vs. lower oxides), their V_2O_5 profile range is useful for our purposes. Their Li/V intensity ratio shows in the 40 nm thin range a variation with sputtering time, therefore sampling depth, Figs. 6 and 7 in [14], which is very similar to our Mn depth profile in Fig. 5. In their Fig. 7, the Li/V intensity ratio decreases from 8 to 4 in the range of 5 nm, and then increases to a ratio of 10–13 at 40 nm thickness, and then decreases again, so as to show a sinusoidal Li concentration profile. Interestingly, Saito et al. [17] observe a constant Li concentration profile in 30 μm thick electrode layers with glow discharge optical emission spectroscopy even after 50,000 cycles of operation. The profiles for the other elements, such as Ni, Co, Al, and carbon were as constant as well. Only at the electrode surface and current collector interface, deviations from constant profile were found (Figs. 2 and 3 in Ref. [15]). Also the Li concentration in LiPON films was virtually constant, at least in the center of the samples, as probed with cold neutron depth profiling by Lamaze et al. [18] on samples thinner than 1 μm. Yang et al. [19] used XPS on a $LiMn_2O_4$ electrode and found that the Li 1s intensity was increased at the electrode surface and decreased consistently towards the current collector in a capacity faded cell.

4. Conclusions

With this sample preparation technique we are able to go beyond the conventional spectroscopy experiments, which allowed only for spatially averaged oxidation states of samples. In the future we will be able to monitor oxidation state variations in samples with a depth resolution of better than 5 μm. This will facilitate studies on the pathogenesis of battery electrodes during charging/discharging and possibly address engineering issues for the electrode design as well. Basically, it should be possible to reproduce depth profiles like the one found in this study by applying mathematical models for the spatial current distribution of realistic porous electrodes [18].

Acknowledgments

This work was supported by the Director, Office of Basic Energy Sciences, Chemical Sciences Division of the U.S. Department of Energy, under Contract DE-AC03-76SF00098. Use of the Advanced Photon Source at Argonne National Laboratory was supported by the U.S. Department of Energy, Office of Science, Office of Basic Energy Sciences, under Contract No. DE-AC02-06CH11357. The ALS is supported by the Director, Office of Science/BES, of the U.S. DoE, # DE-AC02-05CH11231. Financial support for A.B. by the European Commission (MIRG # CT-2006-042095) is acknowledged.

References

[1] A. Claye, J.E. Fischer, Electrochimica Acta 45 (1–2) (1999) 107.
[2] M.C. Tucker, J.A. Reimer, E.J. Cairns, Electrochemical and Solid State Letters 3 (10) (2000) 463.
[3] Y. Shao-Horn, L. Croguennec, C. Delmas, E.C. Nelson, M. O'Keefe, Nature Materials 2 (7) (2003) 464.
[4] A. Braun, H. Wang, J.P. Shim, S.S. Lee, E.J. Cairns, Journal of Power Sources 170 (2007) 173.
[5] A. Braun, H. Wang, U. Bergmann, M.C. Tucker, W. Gu, S.P. Cramer, E.J. Cairns, Journal of Power Sources 112 (1) (2003) 231.
[6] R. Solarska, B.D. Alexander, A. Braun, R. Jurczakowski, G. Fortunato, M. Stiefel, T. Graule, J. Augustynski, Electrochimica Acta, in press, doi:10.1016/j.electacta.2009.12.016.
[7] A. Braun, S. Seifert, P. Thiyagarajan, S.P. Cramer, E.J. Cairns, Electrochemistry Communications 3 (3) (2001) 136.
[8] M.C. Tucker, A. Braun, U. Bergmann, H. Wang, P. Glatzel, J.A. Reimer, S.P. Cramer, E.J. Cairns, in: A. Landgrebe, R.J. Klingler (Eds.), Proceedings of the Workshop on Interfaces, Phenomena and Nanostructures in Lithium Batteries, Argonne National Laboratory, The Electrochemical Society, PV 2000-36, 2000, pp. 68–79.
[9] M.C. Tucker, J.A. Reimer, E.J. Cairns, Journal of the Electrochemical Society 149 (2002) A574.
[10] M.C. Tucker, J.A. Reimer, E.J. Cairns, Journal of the Electrochemical Society 148 (8) (2001) A951–A959.
[11] A. Braun, S. Shrout, A.C. Fowlks, B.A. Osaisai, S. Seifert, E. Granlund, E.J. Cairns, Journal of Synchrotron Radiation 10 (2003) 320.
[12] K. Kanamura, H. Tamura, Z.-I. Takehara, Journal of Electroanalytical Chemistry 333 (1-2) (1992) 127–142.
[13] J. Song, B.-L. Hong, J. Zheng, P. Lin, M.-S. Zheng, Q.-H. Wu, Q.-F. Dong, S.-G. Sun, Applied Physics A, Materials Science & Processing 98 (2010) 455.
[14] C.R. Horne, U. Bergmann, M.M. Grush, R.C.C. Perera, D.L. Ederer, T.A. Callcott, E.J. Cairns, S.P. Cramer, Journal of Physical Chemistry B 104 (2000) 9587.
[15] M.V. Reddy, B. Pecquenard, P. Vinatier, C. Wannek, A. Levasseur, P. Moretto, Nuclear Instruments and Methods in Physics Research Section B: Beam Interactions with Materials and Atoms 246 (2) (2006) 397.
[16] J. Światowska-Mrowiecka, F. Martin, V. Maurice, S. Zanna, L. Klein, J. Castle, P. Marcus, Electrochimica Acta 53 (12) (2008) 4257.
[17] Y. Saito, Md. K. Rahman, Journal of Power Sources 174 (2) (2007) 877.
[18] G.P. Lamaze, H.H. Chen-Mayer, D.A. Becker, F. Vereda, R.B. Goldner, T. Haas, P. Zerigian, Journal of Power Sources 119–121 (2003) 680.
[19] L. Yang, M. Takahashi, B. Wang, Electrochimica Acta 51 (16) (2006) 3228.